Journal of Materials Chemistry A

PAPER

View Article Online
View Journal | View Issue

Cite this: J. Mater. Chem. A, 2014, 2, 3926

AB–MH (Ammonia Borane–Metal Hydride) composites: systematic understanding of dehydrogenation properties

Yuki Nakagawa,*[a] Shigehito Isobe,*[ab] Yudai Ikarashi[a] and Somei Ohnuki[a]

Received 13th November 2013
Accepted 3rd January 2014

DOI: 10.1039/c3ta14670g

www.rsc.org/MaterialsA

Dehydrogenation properties of AB–MH (Ammonia Borane–Metal Hydride, M = K, Na, Li, Ca, Mg, Al) composites were systematically investigated by thermal and mass analyses. The results suggest that the Pauling electronegativity of M, χ_p, is a good indicator to predict the phases of composites, the dehydrogenation temperature and the amount of by-product gases (NH_3 and B_2H_6). The phases of composites were classified by χ_p as follows. MBH_4 was formed for M = K, Na ($\chi_p \leq 0.9$), MNH_2BH_3 was formed for M = Na, Li ($0.9 \leq \chi_p \leq 1.0$) and no new compounds were formed for M = Ca, Mg, Al ($1.0 \leq \chi_p$). The 1st dehydrogenation temperatures of the samples (M = Na, Li, Ca, Mg) were 10–20 °C lower than that of AB itself ($\chi_p \leq 1.2$). The amount of NH_3 was decreased as χ_p increased. On the other hand, the amount of B_2H_6 was decreased as χ_p decreased. The emission of $B_3H_6N_3$ could occur by the reaction of NH_3 and B_2H_6. Finally, AB–$MAlH_4$ (M = Na, Li) composites, which were prepared based on the indicator, showed superior potential as hydrogen storage materials because they did not desorb any by-products NH_3, B_2H_6 and $B_3H_6N_3$.

1. Introduction

Ammonia borane (NH_3BH_3, AB) is an attractive candidate for hydrogen storage media because of its high hydrogen content (19.6 wt%, 0.145 kg L^{-1}).[1–3] It can desorb ~13 wt% of hydrogen below 200 °C.[4–6] The dehydrogenation of AB takes place in three steps within a single equivalent of hydrogen evolved in each step at *ca.* 70–110, 110–200, and 400–900 °C in temperature ramping experiments.[4–6] One of the disadvantages for practical application is the emission of by-product gases such as ammonia (NH_3), diborane (B_2H_6), and borazine ($B_3H_6N_3$). For instance, release of ammonia causes damage to the fuel cell performance even at trace levels.[7] Worse yet, NH_3 and B_2H_6 are harmful for living creatures.[8,9]

The dehydrogenation properties of AB–MH composites have been extensively studied, such as AB–LiH,[10–18] AB–NaH,[10–13,19–21] AB–LiH–NaH,[12] AB–KH,[11,13,14,22] AB–MgH_2,[23,24] AB–CaH_2,[18,23,25] AB–$LiNH_2$,[26] AB–$LiBH_4$,[27] AB–Li_3AlH_6,[28] and AB–$LiNH_2$–$LiBH_4$,[29] in order to improve the dehydrogenation properties of AB. For example, the AB–NaH composite desorbed hydrogen at 80–100 °C without the by-product diborane and borazine.[20,21] The AB–$LiNH_2$ composite desorbed hydrogen as low as 60 °C without the by-products diborane and borazine.[26] However, systematic investigation on AB–MH composites has not been explored. On the other hand, thermodynamical stabilities of $M(BH_4)_n$ and $M(AlH_4)_n$ systems have been systematically investigated by using the Pauling electronegativity of M as an indicator.[30–33] The correlation between the dehydrogenation temperature and the Pauling electronegativity of M was found computationally and experimentally.[30–33] It is of great importance to understand the dehydrogenation properties of AB–MH composites systematically in order to decrease the dehydrogenation temperature and suppress by-product gas emission.

In this study, AB–MH (M = K, Na, Li, Ca, Mg, Al) composites were synthesized by a ball milling method. Phases of AB–MH composites were determined by X-ray diffraction (XRD) analysis and dehydrogenation properties were discussed in terms of dehydrogenation temperature and amounts of hydrogen and by-product gas emissions. From the results, we proposed an indicator to predict the phases of composites, the dehydrogenation temperature and the amount of by-product gas emission (NH_3 and B_2H_6). Finally, we created superior composites according to the indicator and evaluated their dehydrogenation properties.

2. Experimental

The starting materials NH_3BH_3, NaH, LiH, CaH_2, $NaAlH_4$, and $LiAlH_4$ (purity 97%, 55–65% (moistened with oil), 95%, 99.99%, 90%, and 95%, respectively) were purchased from Sigma Aldrich Co. Ltd. MgH_2 (purity 98%) was purchased from Alfa Aesar. These materials were used as-received

[a]Graduate School of Engineering, Hokkaido University, N-13, W-8, Sapporo 060-8278, Japan. E-mail: isobe@eng.hokudai.ac.jp; y-nakagawa@eng.hokudai.ac.jp; Fax: +81-11-706-6772; Tel: +81-11-706-6771

[b]Creative Research Institution, Hokkaido University, N-21, W-10, Sapporo 001-0021, Japan

without any purification. AlH_3 was prepared by the chemical reaction between $LiAlH_4$ and $AlCl_3$ in ether solution.[34] KH was prepared according to ref. 35. All samples were handled in an argon glovebox without exposing samples to air. AB–MH (M = K, Na, Li, Ca, Mg, Al) and AB–$MAlH_4$ (M = Na, Li) composites were prepared by ball-milling under 0.1 MPa Ar with 400 rpm for 30 min, 1.0 MPa H_2 with 300 rpm for 5 min, respectively. Ball-milling processes were performed by using a planetary ball-mill apparatus (Fritsch Pulverisette 7) with 20 stainless steel balls (7 mm in diameter) and 300 mg samples (ball : powder ratio = 70 : 1, by mass). The phase analysis was conducted by powder X-ray diffraction (XRD, PANalytical, X'Pert-Pro with Cu Kα radiation). The dehydrogenation properties were examined by thermal desorption mass spectrometry measurements (TDMS, ULVAC, BGM-102) combined with thermogravimetry and differential thermal analysis (TG-DTA, Bruker, 2000SA). The heating rate was 2 or 5 °C min^{-1} and the helium gas flow rate was 300 mL min^{-1}. TDMS measurements combined with TG-DTA were performed twice for each sample. The amounts of hydrogen and by-product gases were defined by integrating the peaks of mass spectra. The value of integral for by-product gases was normalized by that for hydrogen. Then, the weight loss of each gas was estimated by the total weight loss obtained from TG results. All measurements were immediately performed after synthesizing the AB–MH composite in order to prevent the composite from decomposing.

3. Results and discussion

3.1 Phase analysis of AB–MH composites

Fig. 1 shows the XRD patterns of each AB–MH composite and AB after milling and heating to 200 °C. Broad diffraction peaks around 20° and 27° in all profiles originate from the film and grease to prevent the sample oxidation. A small amount of $(NH_2BH_2)_4$ was observed in the milled AB. This phase was considered as impurity in as-received AB. After heating AB, there were no peaks in the profile, indicating that AB became amorphous. For the AB–NaH composite, peaks were consistent with sodium amidoborane ($NaNH_2BH_3$), which was confirmed by Xiong *et al.*[10] After heating, $NaBH_4$ was confirmed by XRD, which is different from the experimental results of previous investigators.[19–21] One of the possibilities of $NaBH_4$ formation would come from the different milling condition. There are some cases that non-equilibrium phases appear by mechanical ball milling.[36] As described in ref. 20, the formation of BH_4^- ions may occur under the milling condition. For the AB–LiH composite, peaks were consistent with lithium amidoborane–ammonia borane ($LiNH_2BH_3 \cdot NH_3BH_3$). This was the intermediate phase during the synthesis of $LiNH_2BH_3$, which was confirmed by Wu *et al.*[17] Thus, metal amidoborane (MNH_2BH_3 (M = Na, Li)) was confirmed after milling for M = Na, Li. For the AB–KH composite, KBH_4 was observed instead of potassium amidoborane (KNH_2BH_3) after milling. The wet chemical synthesis of KNH_2BH_3 by stirring KH and AB in benzene for 2 days suggests that a lower rotation speed and longer time of ball milling enables generation of KNH_2BH_3.[22]

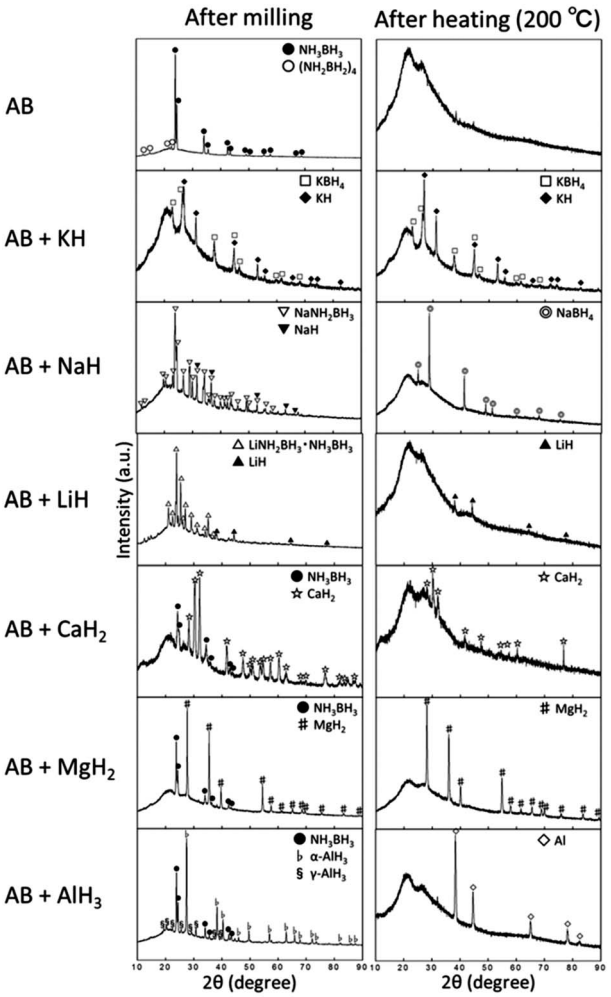

Fig. 1 Powder X-ray diffraction (XRD) profiles of AB–MH (M = K, Na, Li, Ca, Mg, Al) composites and AB after milling and heating to 200 °C.

In cases of AB–MH (M = Ca, Mg, Al) composites, no new compounds were observed after milling. Only AB and each MH phase were observed. It was reported that more than 6 hours milling by using a shaker mill can generate $Ca(NH_2BH_3)_2$.[25] However, synthesis of $Mg(NH_2BH_3)_2$ by ball milling was unsuccessful.[18] After heating, only each MH phase was observed for M = Mg, Ca. These results are in good agreement with previous reports.[23,24] In the case of M = Al, Al was observed after heating, which indicated that AlH_3 desorbed hydrogen below 200 °C. From Fig. 1, we described the crystalline phases of AB–MH composites according to the Pauling electronegativity of M, χ_p, in Table. 1. The previous study about the stability of $M(NH_2BH_3)_n$ by the computational method indicates that electronegativity is a good indicator to understand the stability generally.[13] As shown in Table 1, MBH_4 was formed for M = K, Na ($\chi_p \leq 0.9$), MNH_2BH_3 was formed for M = Na, Li ($0.9 \leq \chi_p \leq 1.0$) and no new compounds were formed for M = Ca, Mg, Al ($1.0 \leq \chi_p$). This suggests that the trend of the phases of AB–MH composites follows the trend of χ_p. MH tends to cause the reaction with AB faster when χ_p decreases.

Table 1 Phases of AB–MH composites classified by the Pauling electronegativity of M. Decomposition temperature is the temperature at which crystalline phases after heating to 200 °C (KBH_4, $NaBH_4$, LiH, CaH_2, and MgH_2) desorb hydrogen. The peak dehydrogenation temperature in mass spectra was described. The heating rate was 5 °C min^{-1}

MH	KH	NaH	LiH	CaH_2	MgH_2	AlH_3
Pauling electronegativity χ_p of M	0.8	0.9	1.0	1.0	1.2	1.5
Crystalline phases after milling	KBH_4	$NaNH_2BH_3$	$LiNH_2BH_3 \cdot NH_3BH_3$	CaH_2	MgH_2	AlH_3
Crystalline phases after heating (200 °C)	KBH_4	$NaBH_4$	LiH	CaH_2	MgH_2	Al
Decomposition temperature/°C	425	400	555	627	446	n/a

3.2 Dehydrogenation properties of AB–MH composites

Fig. 2 shows the dehydrogenation temperatures of AB–MH (M = Na, Ca, Li, Mg, Al) composites below 200 °C. The results of the AB–KH composite were not plotted because it did not desorb any gases during heating below 200 °C. The 1st and 2nd dehydrogenation peak temperatures in mass spectra are plotted in Fig. 2(a) and (b), respectively. The dashed lines show the temperature of milled AB. As shown in Fig. 2(a), 1st temperatures for M = Na, Li, Ca, Mg ($\chi_p \leq 1.2$) were decreased by 10–20 °C as compared with milled AB. These results are in good agreement with other results.[10,23,24] The 1st temperature for M = Al was not changed as milled AB. It is interesting to note that this trend is opposite to the trend in the dehydrogenation temperatures of $M(BH_4)_n$ and $M(AlH_4)_n$.[30–33] The 2nd temperatures for M = Ca, Mg, Al were correlated with the electronegativity of M as shown in Fig. 2(b). It is difficult to compare the whole results of temperatures because phases are different between those for M = Na, Li and those for M = Ca, Mg, Al. The AB–CaH_2 composite showed the lowest temperature of all the 2nd dehydrogenation temperatures. The dehydrogenation from AB–MH composites could be promoted by the solid-phase interaction between AB and MH. This interaction would affect the intramolecular N–H, B–H and B–N chemical bonds and intermolecular dihydrogen bond.

The amounts of hydrogen and by-product gases of AB–MH composites were investigated by TG-MASS. Fig. 3(a) shows the estimated weight losses of hydrogen and by-product gases below 200 °C. Milled AB desorbed by-product gases more than 60%, indicating the substantial amount of by-product gas emission. All the AB–MH composites showed by-product gas emission of 6–18%, suggesting that most of the by-product gases were suppressed. Fig. 3(b) shows the hydrogen purity of

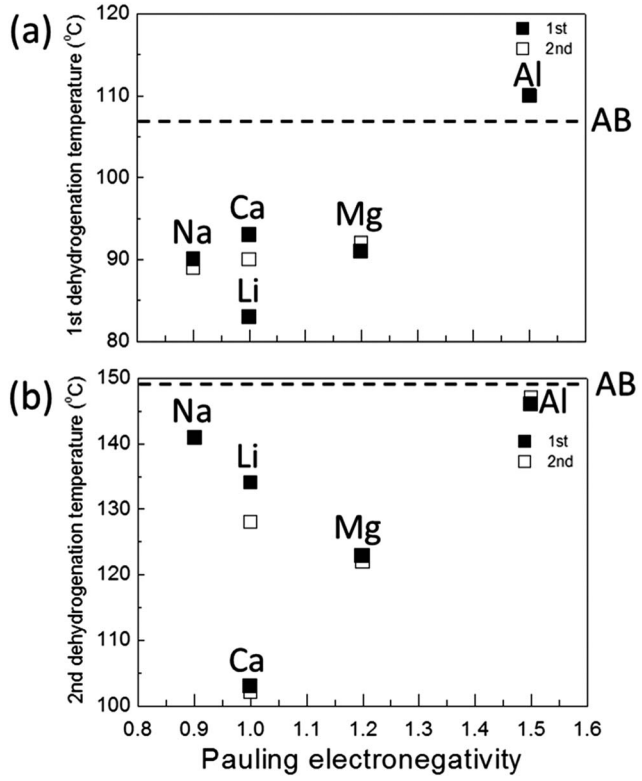

Fig. 2 Dehydrogenation temperatures of AB–MH composites below 200 °C classified by the Pauling electronegativity of M; (a) 1st peak temperatures and (b) 2nd peak temperatures. The heating rate was 2 °C min^{-1}. The black square symbols show the results of the 1st measurement and the white square symbols show those of the 2nd measurement.

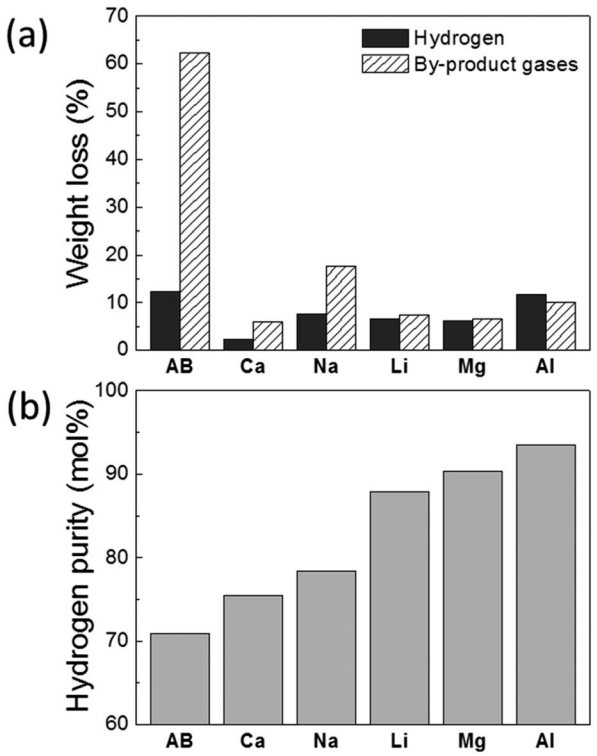

Fig. 3 (a) Weight losses of hydrogen and by-product gases and (b) hydrogen purity of AB–MH composites below 200 °C. The heating rate was 2 °C min^{-1}.

AB–MH composites. A purity of about 90% was obtained for M = Li, Mg, Al. On the other hand, the purity for M = Na, Ca was only less than 80%. In order to investigate the content of by-product gases, we estimated the amounts of by-product gases of NH_3, B_2H_6 and $B_3H_6N_3$. Fig. 4 shows the amounts of by-product gases of AB–MH composites. NH_3, B_2H_6 and $B_3H_6N_3$ were analysed by mass spectrometry. The dashed line shows the amount of milled AB. As shown in Fig. 4(a), the amount of NH_3 was decreased as χ_p increased. The AB–AlH_3 composite almost suppressed the emission of NH_3. On the other hand, the amount of B_2H_6 was decreased as χ_p decreased as shown in Fig. 4(b). AB–MH (M = Na, Li, Ca ($\chi_p \leq 1.0$)) composites completely suppressed B_2H_6. Comparing the results of Fig. 3(b), it was found that the low hydrogen purity for M = Na, Ca was ascribed to a large amount of NH_3 emission. The emission process of NH_3 in the $NaNH_2BH_3$ system was reported by Fijałkowski *et al.*,[20] which explained the fact that the formation and decomposition of the ionic salt caused the emission. The ionic radius of M^{n+} seems to be correlated with the emission of NH_3. The ionic radii of Na^+ (102 pm) and Ca^{2+} (100 pm) are different from those of Li^+ (76 pm), Mg^{2+} (72 pm), and Al^{3+} (54 pm).[37] The trend in the amount of B_2H_6 was similar to that in the case of $M(BH_4)_n$. In the case of $M(BH_4)_n$, those for $\chi_p \leq 1.5$ suppressed the emission of B_2H_6.[30] The previous study showed diammoniate of diborane (DADB), $[(NH_3)_2BH_2]^+[BH_4]^-$, an ionic isomer of AB, is formed during the induction period before dehydrogenation of AB.[38] If DADB is regarded as a kind of borohydride, the emission process of B_2H_6 in AB is considered to be similar to that in $M(BH_4)_n$. Further investigations are needed to clarify the suppression mechanisms of NH_3 and B_2H_6 emission in AB–MH composites. Fig. 4(c) shows that only the AB–MgH_2 composite desorbed $B_3H_6N_3$. The emission of $B_3H_6N_3$ may correlate with the emission of NH_3 and B_2H_6. $B_3H_6N_3$ can be generated by the reaction between NH_3 and B_2H_6 with a molar ratio of 2 : 1.[39] The AB–MgH_2 composite desorbed NH_3 and B_2H_6, then they would react to form $B_3H_6N_3$. In the other composites, emission of either NH_3 or B_2H_6 was suppressed, which would result in the suppression of $B_3H_6N_3$ emission. As a result, χ_p would be a good indicator to predict the dehydrogenation temperatures and the amounts of by-product gases. We summarized the dehydrogenation properties of composites in Fig. 5. Fig. 5 shows the amounts of hydrogen desorbed below 200 °C *versus* dehydrogenation temperatures. The AB–CaH_2 composite showed the lowest dehydrogenation temperature and the AB–AlH_3 composite showed the largest amount of hydrogen of all the composites. However, it was indicated that there were no materials fulfilling large amounts of hydrogen desorbed at low temperatures. In order to accomplish these requirements, further investigations, *e.g.* combining AB with more than two metal hydrides, will be needed.

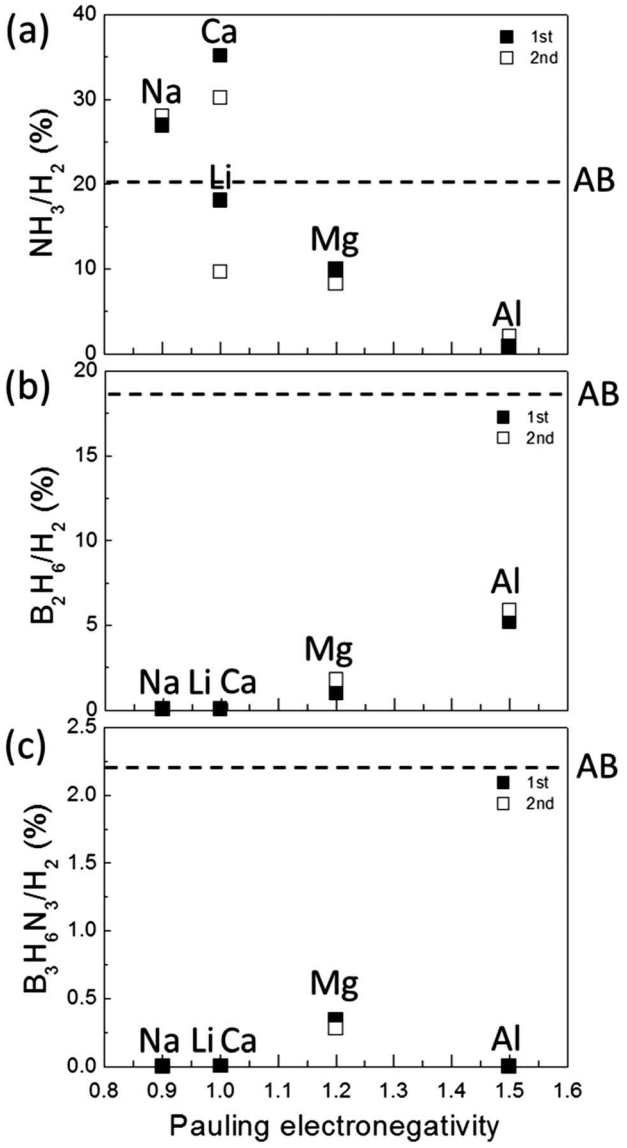

Fig. 4 The amounts of by-product gases desorbed by AB–MH composites classified by the Pauling electronegativity of M; (a) ammonia (NH_3), (b) diborane (B_2H_6), and (c) borazine ($B_3H_6N_3$). The heating rate was 2 °C min^{-1}. The black square symbols show the results of the 1st measurement and the white square symbols show those of the 2nd measurement.

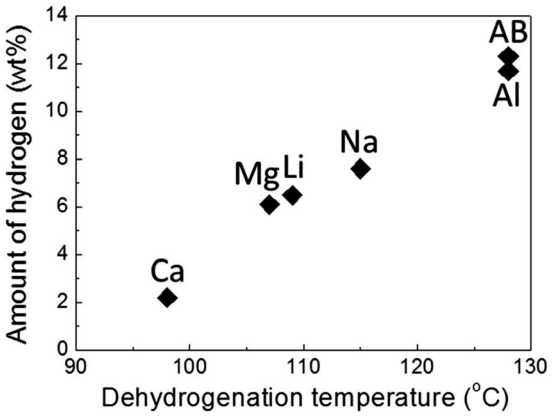

Fig. 5 The amounts of hydrogen desorbed by AB–MH composites below 200 °C *versus* dehydrogenation temperatures. The average temperatures between the 1st and 2nd temperatures were plotted. The heating rate was 2 °C min^{-1}.

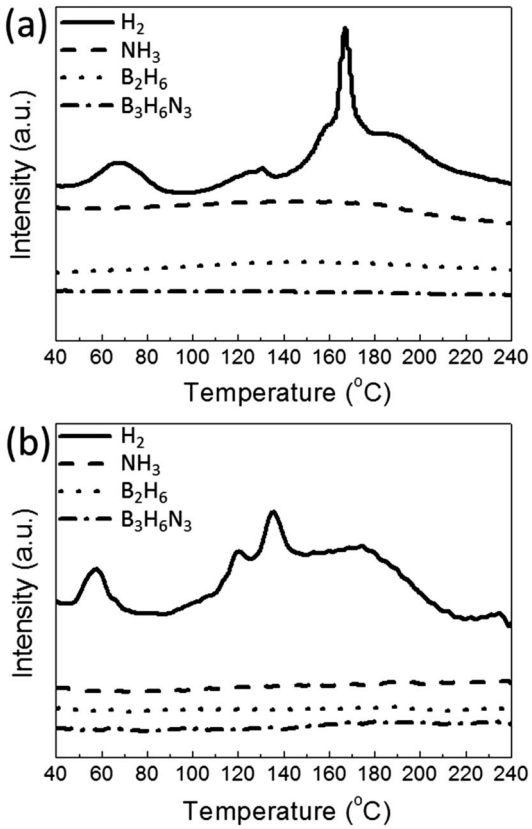

Fig. 6 The mass spectra of the (a) AB–$NaAlH_4$ composite and (b) AB–$LiAlH_4$ composite. The heating rate was 5 °C min^{-1}.

3.3 Creation of AB–MH composites based on the indicator

On the basis of the indicator described in Section 3.2, we created superior AB–MH composites. As shown in Fig. 4, the emissions of NH_3 and B_2H_6 were suppressed by combining with AlH_3 and NaH (LiH), respectively. Therefore, we thought the idea of combining $MAlH_4$ (M = Na, Li) with AB because $MAlH_4$ (M = Na, Li) is the compound consisting of MH (M = Na, Li) and AlH_3. The milling conditions of AB–$MAlH_4$ composites are described in the Experimental part. The milling time of 5 min would be appropriate because milling for 30 min resulted in the decomposition of composites during milling. The mass spectra of AB–$NaAlH_4$ and AB–$LiAlH_4$ composites are shown in Fig. 6. It is interesting that both composites did not desorb NH_3, B_2H_6 and $B_3H_6N_3$ at all within the accuracy of our apparatus. Only hydrogen gas was desorbed. About 4 wt% of hydrogen was desorbed below 240 °C in both composites. The suppression of by-product gas emission was also confirmed in AB–Li_3AlH_6 composites.[28] Thus, AB–$MAlH_4$ (M = Na, Li) composites showed superior potential as hydrogen storage materials. Investigations of the reaction processes of both composites are currently in progress.

4. Conclusion

In order to decrease the dehydrogenation temperature and suppress by-product gas emission, we investigated the phases and dehydrogenation properties of AB–MH composites prepared by ball-milling. MBH_4 was formed for M = K, Na ($\chi_p \leq 0.9$), MNH_2BH_3 was formed for M = Na, Li ($0.9 \leq \chi_p \leq 1.0$) and no new compounds were formed for M = Ca, Mg, Al ($1.0 \leq \chi_p$). 1st dehydrogenation temperatures for M = Na, Li, Ca, Mg ($\chi_p \leq 1.2$) were decreased by 10–20 °C as compared with the milled one. The amount of NH_3 was decreased as electronegativity increased. The AB–AlH_3 composite almost suppressed the emission of NH_3. On the other hand, the amount of B_2H_6 was decreased as electronegativity decreased. AB–MH (M = Na, Li, Ca ($\chi_p \leq 1.0$)) composites completely suppressed B_2H_6. $B_3H_6N_3$ emission was observed for M = Mg. The emission could be occurred by the reaction between NH_3 and B_2H_6. These results suggested that the Pauling electronegativity of M, χ_p, is a good indicator to predict the phases of composites, dehydrogenation temperature and the amount of by-product gas emission (NH_3 and B_2H_6). AB–$MAlH_4$ (M = Na, Li) composites, which were prepared based on the indicator, showed superior potential as hydrogen storage materials because they did not desorb any by-products NH_3, B_2H_6 and $B_3H_6N_3$. These results would be helpful for clarifying the improvement mechanism of dehydrogenation properties and designing new hydrogen storage materials.

Notes and references

1 F. H. Stephens, V. Pons and R. T. Baker, *Dalton Trans.*, 2007, **25**, 2613–2626.
2 C. W. Hamilton, R. T. Baker, A. Staubitz and I. Manners, *Chem. Soc. Rev.*, 2009, **38**, 279–293.
3 P. Wang and X. Kang, *Dalton Trans.*, 2008, **40**, 5400–5413.
4 M. G. Hu, R. A. Geanangel and W. W. Wendlandt, *Thermochim. Acta*, 1978, **23**, 249–255.
5 V. Sit, R. A. Geanangel and W. W. Wendlandt, *Thermochim. Acta*, 1987, **113**, 379–382.
6 G. Wolf, J. Baumann, F. Baitalow and F. P. Hoffmann, *Thermochim. Acta*, 2000, **343**, 19–25.
7 N. Rajalakshmi, T. T. Jayanth and K. S. Dhathathreyan, *Fuel Cells*, 2004, **3**, 177–180.
8 International Chemical Safety Cards, ICSC number: 0414.
9 International Chemical Safety Cards, ICSC number: 0432.
10 Z. Xiong, C. K. Yong, G. Wu, P. Chen, W. Shaw, A. Karkamkar, T. Autrey, M. O. Jones, S. R. Johnson, P. P. Edwards and W. I. F. David, *Nat. Mater.*, 2008, **7**, 138–141.
11 A. T. Luedtke and T. Autrey, *Inorg. Chem.*, 2010, **49**, 3905–3910.
12 Y. Zhang, K. Shimoda, T. Ichikawa and Y. Kojima, *J. Phys. Chem. C*, 2010, **114**, 14662–14664.
13 Y. Zhang and C. Wolverton, *J. Phys. Chem. C*, 2012, **116**, 14224–14231.
14 K. Shimoda, K. Doi, T. Nakagawa, Y. Zhang, H. Miyaoka, T. Ichikawa, M. Tansho, T. Shimizu, A. K. Burrell and Y. Kojima, *J. Phys. Chem. C*, 2012, **116**, 5957–5964.
15 Z. Yang, Y. Wang, J. Liang and J. Chen, *Mater. Trans.*, 2011, **52**, 651–653.

16 C. Wu, G. Wu, Z. Xiong, W. I. F. David, K. R. Ryan, M. O. Jones, P. P. Edwards, H. Chu and P. Chen, *Inorg. Chem.*, 2010, **49**, 4319–4323.
17 C. Wu, G. Wu, Z. Xiong, X. Han, H. Chu, T. He and P. Chen, *Chem. Mater.*, 2010, **22**, 3–5.
18 H. Wu, W. Zhou and T. Yildirim, *J. Am. Chem. Soc.*, 2008, **130**, 14834–14839.
19 Z. Xiong, G. Wu, Y. S. Chua, J. Hu, T. He, W. Xu and P. Chen, *Energy Environ. Sci.*, 2008, **1**, 360–363.
20 K. J. Fijałkowski and W. Grochala, *J. Mater. Chem.*, 2009, **19**, 2043–2050.
21 K. Shimoda, Y. Zhang, T. Ichikawa, H. Miyaoka and Y. Kojima, *J. Mater. Chem.*, 2011, **21**, 2609–2615.
22 H. V. K. Diyabalanage, T. Nakagawa, R. P. Shrestha, T. A. Semelsberger, B. L. Davis, B. L. Scott, A. K. Burrell, W. I. F. David, K. R. Ryan, M. O. Jones and P. P. Edwards, *J. Am. Chem. Soc.*, 2010, **132**, 11836–11837.
23 Y. Zhang, K. Shimoda, H. Miyaoka, T. Ichikawa and Y. Kojima, *Int. J. Hydrogen Energy*, 2010, **35**, 12405–12409.
24 X. Kang, L. Ma, Z. Fang, L. Gao, J. Luo, S. Wang and P. Wang, *Phys. Chem. Chem. Phys.*, 2009, **11**, 2507–2513.
25 F. Leardini, J. R. Ares, J. Bodega, M. J. Valero-Pedraza, M. A. Bañares, J. F. Fernández and C. Sánchez, *J. Phys. Chem. C*, 2012, **116**, 24430–24435.
26 K. R. Graham, T. Kemmitt and M. E. Bowden, *Energy Environ. Sci.*, 2009, **2**, 706–710.
27 J. Luo, H. Wu, W. Zhou, X. Kang, Z. Fang and P. Wang, *Int. J. Hydrogen Energy*, 2012, **37**, 10750–10757.
28 G. Xia, Y. Tan, X. Chen, Z. Guo, H. Liu and X. Yu, *J. Mater. Chem. A*, 2013, **1**, 1810–1820.
29 J. Luo, X. Kang and P. Wang, *Int. J. Hydrogen Energy*, 2013, **38**, 4648–4653.
30 Y. Nakamori, K. Miwa, A. Ninomiya, H. W. Li, N. Ohba, S. Towata, A. Züttel and S. Orimo, *Phys. Rev. B: Condens. Matter Mater. Phys.*, 2006, **74**, 045126.
31 Y. Nakamori, H. W. Li, K. Kikuchi, M. Aoki, K. Miwa, S. Towata and S. Orimo, *J. Alloys Compd.*, 2007, **446–447**, 296–300.
32 T. Matsunaga, F. Buchter, K. Miwa, S. Towata, S. Orimo and A. Zuttel, *Renewable Energy*, 2008, **33**, 193–196.
33 J. Graetz, *Chem. Soc. Rev.*, 2009, **38**, 73–82.
34 F. M. Brower, N. E. Matzek, P. F. Reigler, H. W. Rinn, C. B. Roberts, D. L. Schmidt, J. A. Snover and K. Terada, *J. Am. Chem. Soc.*, 1976, **98**, 2450–2453.
35 H. Yamamoto, H. Miyaoka, S. Hino, H. Nakanishi, T. Ichikawa and Y. Kojima, *Int. J. Hydrogen Energy*, 2009, **34**, 9760–9764.
36 C. Suryanarayana, *Prog. Mater. Sci.*, 2001, **46**, 1–184.
37 L. Pauling, *The Nature of the Chemical Bond*, Cornell University Press, Ithaca, NY, 3rd edn, 1960.
38 A. C. Stowe, W. J. Shaw, J. C. Linehan, B. Schmid and T. Autrey, *Phys. Chem. Chem. Phys.*, 2007, **9**, 1831–1836.
39 E. Wiberg and A. Bolz, *Berichte*, 1940, **73**, 209–232.